Cascading quantum light-matter interfaces with minimal interconnection losses

Mehdi Namazi, Thomas Mittiga, Connor Kupchak, and Eden Figueroa

Phys. Rev. A **92**, 033846 — Published 24 September 2015

DOI: 10.1103/PhysRevA.92.033846

Cascading Quantum Light-Matter Interfaces with Minimal Interconnection Losses

Mehdi Namazi, Thomas Mittiga, Connor Kupchak and Eden Figueroa[1]

[1]*Department of Physics and Astronomy, Stony Brook University, New York 11794-3800, USA*

The ability to interface multiple optical quantum devices is a key milestone towards the development of future quantum information processors and networks. One of the requirements for any of their constituent elements will be cascadability, i.e. the ability to drive the input of a device using the output of another one. Here, we report the cascading of quantum light-matter interfaces by storing few-photon level pulses of light in warm vapor followed by the subsequent storage of the retrieved field onto a second ensemble. We demonstrate that by using built-in purification mechanisms in the sequential storage, the final signal-to-background ratio can remain greater than one for weak pulses containing eight input photons on average.

PACS numbers: 42.50.Ex, 42.50.Gy

Any machine can be defined as a device composed of many constituents with their own specific functions but when interfaced together, are designed to carry out a much greater task. This same description would hold true for a quantum information processor. Given the recent success in the manipulation of individual quantum systems [1, 2], the next step towards the realization of such a quantum machine is the interconnection between multiple quantum network components [3–6].

Ideally these networks will have quantum nodes producing outputs suited for driving (as inputs) succeeding quantum nodes. This is the concept of quantum cascadability [7], and it is a necessary attribute to share and process entanglement in many quantum computer architectures and quantum communication protocols [8–13]. This concept has been widely implemented in setups based upon the interconnecting of quantum state sources and memories [14, 15]. However, protocols or operations interconnecting sources and multiple devices (i.e. memories) in a sequential manner have been primarily unexplored, particularly due to the severe losses incurred to purify the output of the system after each process.

Of the existing multi-device protocols, many will be reliant on operational quantum memories [16], and furthermore on the functionality to have quantum memories that efficiently interface with the output of a preceding memory while incurring minimal propagation losses between systems. More specifically, cascading of quantum memories are necessary for certain one-way quantum computing schemes [17], the implementation of conditional CZ gates [18] and generating multi-mode quantum states [19]. Built on recent successes [20–23], we consider room temperature atomic vapor memories as the elements that comprise a series of cascadable devices that could form the foundation of a quantum network. Room temperature systems are a promising direction, as they can offer a relatively inexpensive experimental overhead while also having strong light matter interaction at the single photon level [24–26].

Here we present the cascaded storage of weak optical pulses containing a few photons on average in two, independent room-temperature quantum light-matter interfaces in the conditions of electromagnetically induced transparency (EIT).

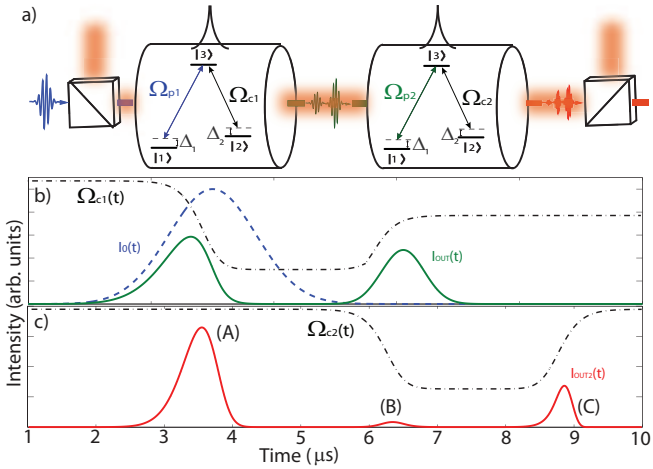

FIG. 1: (color online) (a) Concept of the cascaded storage with two light-matter interfaces. (b) First storage: Input pulse (blue dotted line), control field 1 time sequence (black dotted line) and retrieved light signal (solid green line) as obtained by simulation. (c) Second storage: control field 2 time sequence (dotted black lines, notice the time delay with respect to control field 1) and cascaded retrieved signal (solid red line).

In order to utilize EIT for optical storage, we require atomic systems exhibiting a Λ-energy level scheme. In a cascaded optical storage procedure, the Λ-level scheme of the first atomic ensemble can be characterized by the interaction with two laser fields, Ω_{p1} (probe) and Ω_{c1} (control), with one-photon detunings Δ_1 and Δ_2 respectively (see Fig. 1). The output of this system will be the input to the second ensemble characterized by the interaction with two laser fields, Ω_{p2} (retrieved probe coming from system 1) and Ω_{c2} (control). We assume the detunings of both systems to be identical.

This optical storage can be understood using the Hamiltonian which describes the atom-field coupling in

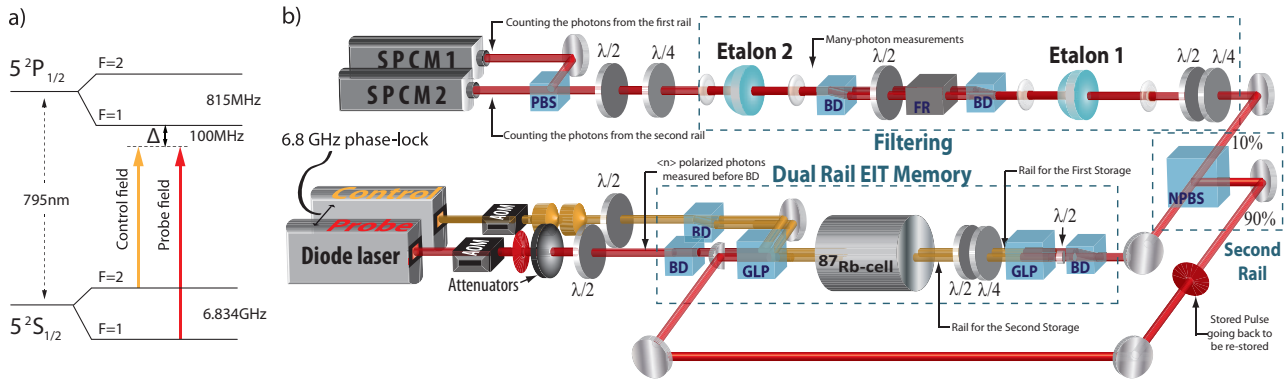

FIG. 2: (color online) (a) Atomic level scheme and EIT configuration used in both memories. (b) Experimental setup for successive storage of pulses at the few-photon level, including the stages of control-filtering. AOM: Acousto-optical modulator; BD: Beam displacer; GLP: Glan-Laser-Polarizer; FR: Faraday rotator; SPCM: Single-Photon-Counting-Module; L: Lens; M: Mirror; NPBS: Non-Polarizing Beam Splitter. Probe: red beam paths; control: yellow beam paths. The NPBS transmits 10% of the first stored pulse through the filtering system to be characterized and sends 90% back to the second rail for a successive storage.

a rotating frame. This is given by:

$$\hat{H} = \Delta_1\hat{\sigma}_{33}+(\Delta_1-\Delta_2)\hat{\sigma}_{22}+\Omega_{p1}E_{p1}(z,t)\hat{\sigma}_{31}+\Omega_{c1}(t)\hat{\sigma}_{32}+h.c. \quad (1)$$

where $\hat{\sigma}_{ij} = |i\rangle\langle j|, i,j = 1,2,3$ are the atomic raising and lowering operators for $i \neq j$, and the atomic energy-level population operators for $i = j$ and $E_{p1}(z,t)$ is the normalized electric field amplitude of the probe. The dynamics of the first storage event can be obtained numerically by solving the master equation for the atom-light system density operator together with the Maxwell-Bloch equation that contains the impact of the atomic polarization on the electromagnetic field for an atomic sample of finite-length L.

$$\dot{\hat{\rho}} = -i[\hat{H},\hat{\rho}] + \sum_{m=1,2}\Gamma_{3m}(2\hat{\sigma}_{m3}\rho\hat{\sigma}_{3m} - \hat{\sigma}_{33}\hat{\rho} - \hat{\rho}\hat{\sigma}_{33}) \quad (2)$$

$$\partial_z E_{p1}(z,t) = i\frac{\Omega_{p1}N}{c}\langle\hat{\sigma}_{31}(z,t)\rangle. \quad (3)$$

Here Γ_{31} and Γ_{32} are the decay rates of the excited level $|3\rangle$ to the ground states $|1\rangle$ and $|2\rangle$ respectively, c is the speed of light in vacuum and N the number of atoms participating in the ensemble. Using initial conditions of $\Omega_{C1}(t)$ and $E_p(0,t) = E_o(t)$ (the original probe pulse shape) allows us to solve this set of equations and calculate the expected retrieved pulse shape $E_{OUT}(t) = E_{p1}(L,t)$. Once we know $E_{OUT}(t)$, we can propagate this result to serve as the input of the second Λ-system and similarly calculate the result of the cascaded storage procedure $E_{OUT2}(t)$.

In Figure 1b, we plot the simulation of the first storage and retrieval event using $\Omega_{c1}(t)$ (black dotted line in Fig. 1b) and $E_p(0,t) = E_o(t)$ (blue dotted line in Fig. 1b) as the control and probe inputs respectively. The result for $E_{OUT}(t) = E_{p1}(L,t)$ (Fig. 1b, in intensity, solid green light) contains a portion of the input pulse that is not stored and transmitted (left peak) followed by the retrieved signal due to the storage (right peak). Figure 1c shows the simulation of the second storage and retrieval event using $\Omega_{c2}(t)$ (dotted black line in Fig. 1c) and $E_{OUT}(t)$ as the control and probe field inputs respectively.

The resultant cascaded stored signal contains three distinct peaks (Fig. 1c in intensity, solid red line), an initial probe leakage from the first storage procedure (A, leftmost peak), a second small leakage from the second procedure (B, middle peak) and a third peak whose timing matches that of when the second control field is switch on again (C, right most peak). This final peak corresponds to a portion of the probe field that has been sequentially stored and retrieved in two independent light matter interfaces. In our simulations we have used $\Gamma_{31} = \Gamma_{32} = 3.0\pi * 10^6 s^{-1}, N \sim 10^{10}$ atoms and $L = 7cm$.

In order to implement the cascading procedure experimentally, we employed two external-cavity diode lasers as light sources, phase-locked at 6.8 GHz to resonantly couple a Λ-configuration. The probe field frequency is stabilized to the $5S_{1/2}F = 1 \rightarrow 5P_{1/2}F' = 1$ transition at a wavelength of 795 nm (red detuning Δ=100 MHz) while the control field interacts with the $5S_{1/2}F = 2 \rightarrow 5P_{1/2}F' = 1$ transition (Fig. 2a).

Our setup is adapted from our prior dual-rail memory experiment [26], where each rail now serves as a distinct optical memory within a single vapor cell containing isotopically pure Rb 87. The temporal shaping of the probe and the control fields are independently controlled with acousto-optical modulators. A polarization beam displacer is used to create a dual-rail set-up for the control field where each rail is mode matched to the respective probe via a Glan-laser polarizer (see Fig. 2b). An initial 100 μW-peak input pulse of 1 μs duration horizontally polarized is sent through the first rail (solid blue line in

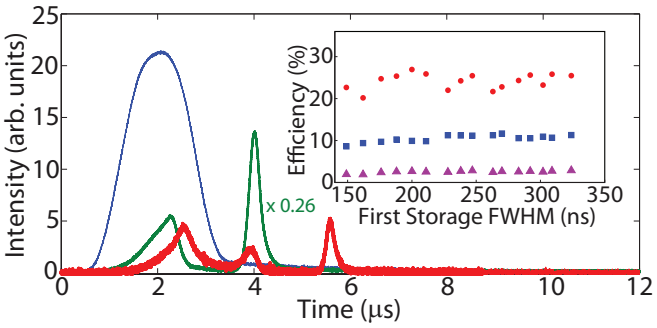

FIG. 3: (color online) Successive storage of classical pulses. Blue: input pulse; Green: rail 1 single storage signal; Red: rail 2 cascaded storage signal. The green line is scaled by a factor 0.26 to account for different propagation losses after the first and second rails. Inset: dependency of storage efficiencies on the full-with half maximum of the Gaussian shaped retrieved field for the first storage. Blue: efficiency of the first storage η_1; Red: efficiency of the second storage η_2; Purple: overall efficiency of cascaded storage procedures η_T.

Fig. 3). Using one of the control fields, the probe pulse is stored for a duration of 1 μs. For the first storage, we apply a temporal modulation to the control field used for retrieval, which allows tuning of the instantaneous group velocity of the retrieved excitation and consequently the tailoring of its temporal shape. We use a near Gaussian temporal profile (see 2nd peak of solid green line in Fig. 3) to yield an efficiency (η_1) of $\sim 12\%$.

The retrieved pulse is transmitted through a polarizer followed by a beam displacer for recombination to a single beam path. After this step, a 90/10 beam splitter is used to send the majority of the retrieved photons back to the front of the vapor cell (see Fig. 2) where a pick-off mirror sends the signal through the second rail. The timing of control field 2 is matched to the retrieval of the first memory for the second storage sequence. After the second beam displacer, the signals from the first and second-rail are matched to the same beam path, albeit with orthogonal polarizations which permits independent measurements. The signals transmitted through the 90/10 beam splitter continue through a temperature-controlled etalon and a polarization independent Faraday-isolator to remove the remnants of the control fields. At this point, the classical-level signals are detected in a photo-detector (not shown in Fig. 2). The signals from the second rail (blue and red in Fig. 3) are 3.9 times smaller than those from the first (green in Fig. 3) due to propagation losses and mismatched etalon coupling efficiencies. As shown in Figure 3 (red line), the resultant cascaded stored signal has three peaks as was predicted by our simulations.

To maximize the efficiency of the cascaded storage (η_T), we modify the duration of control field 1 which also affects the temporal length of the retrieved probe field. This has a significant effect on η_T, as the optimal bandwidth of the retrieved pulse resembles the EIT bandwidth exhibited by the vapor cell. A total storage efficiency of $\sim 3\%$ is obtained when the duration of the control field for the first retrieval is 300ns. The efficiency of the second storage event is independently verified to be $\eta_2 \sim 25\%$. We emphasize that the increase in efficiency from η_1 to η_2 is a direct beneficial effect of the spectral shaping of the photons in the output of the first memory.

We now turn our attention to operating our system at the few-photon level. Specifically, we are interested in benchmarking the behaviour of the complete optical storage network and determine the parameters needed to obtain a cascaded retrieved signal that is at the same level of the background produced by the experiment, i.e. signal-to-background ratio (SBR) of 1.

A trace of the input state is shown in Figure 4 (solid green line, from 1 to 2 μs) for an input mean photon number ~ 8. In order to sufficiently extinguish the large number of photons coming from the control fields, we add a second filtering etalon to the setup of the previous measurement. Overall, the complete filtering setup achieves 154 dB of control field suppression, including the 90/10 beam splitter, while yielding a total probe field transmissions of 0.44% and 0.22% for the first and second rails respectively, to generate an effective, control/probe suppression ratio of about 130 dB. As discussed before, the setup permits measurement of the storage in the first rail (see SPCM 1 in Fig. 2) or the cascaded storage from the second rail (see SPCM 2 in Figure 2).

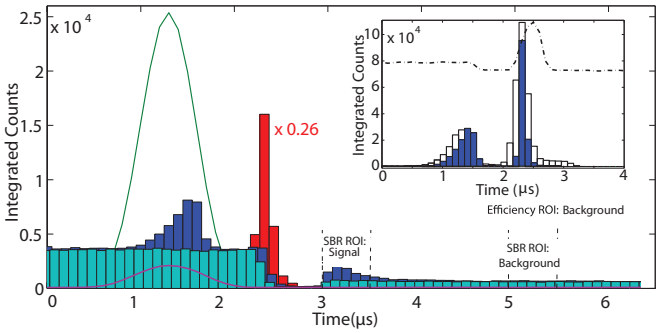

FIG. 4: (color online) Cascaded optical storage for input pulses containing eight photons per pulse on average. Green: input pulse (measured in SPCM 2); Purple: absorbed pulse (measured in SPCM 2); Red: retrieved pulse after first storage (measured in SPCM 1 scaled by a factor 0.26); Blue: retrieved signal after cascaded storage procedure (with background, measured in SPCM 2); Light blue: background-only measurement. Inset: The effect of reshaping the control field for the optical retrieval in the first rail. Storage using on/off modulation of control field 1 (blue bars) and storage counts obtained with a temporally modulated control field 1 (green bars). The temporal shape of the control field 1 is indicated by the dotted-black line.

To determine the total storage efficiency (η_1) in the first rail, we integrate the number of counts over the region of interest (ROI) corresponding to the retrieved pulse (from 2 to 2.5 μs in the inset of Fig. 4) and subtract the number of counts from a signal-free measurement of the background over the same ROI. The magnified

background shape of the control field is included (dashed black line in the inset of Fig. 4) as a guide to the eye. The storage efficiency is then calculated by comparing this difference in counts to the total counts of the probe pulse transmitted (in rail 1) through the filtering system without atomic interaction. The signal to background ratio is obtained using the counts integrated over the ROI in the storage histogram (signal+background) and the number of counts over a signal-free region in the same histogram (background). The SBR is then calculated as [(signal+background)-(background)]/(background).

As shown in the inset of Figure 4, there is a considerable effect on η_1 by using a temporal shaping of the control field for retrieval (white bars), as compared to an experiment with an on/off control field (blue bars). We find a maximum signal-to-background ratio of 13 and an efficiency of 14.6% (see red histogram in Fig. 3). The majority of the photons retrieved from the first memory are sent to the second rail *together with any photons from the first control field* without passing through the filtering setup. This important step allows to reduce the propagation losses by more than 90 % by avoiding the use of additional purification optics in between the memories. We find that after propagation losses (including the routing beam splitter and interconnecting losses from the first to second rail of 53.4%), the mean photon number of the probe field at the input of the second memory is 0.6 photons compared to $\sim 10^8$ photons per pulse from the background. The probe photons are re-stored and then retrieved using the second control field (see dark blue histogram in Fig. 4). For comparison, we also show the counts recorded when the input has been blocked (see light blue bars in Fig. 4).

The cascaded storage signal has a SBR of 1.2. Using a similar procedure to the one described previously, we measure the overall efficiency of the cascaded storage (using a ROI in the interval from 3 to 3.5 μs in Figure 4) to be $\eta_T = 2.9\%$. The efficiency of the second memory η_2 was found to be 19.7%.

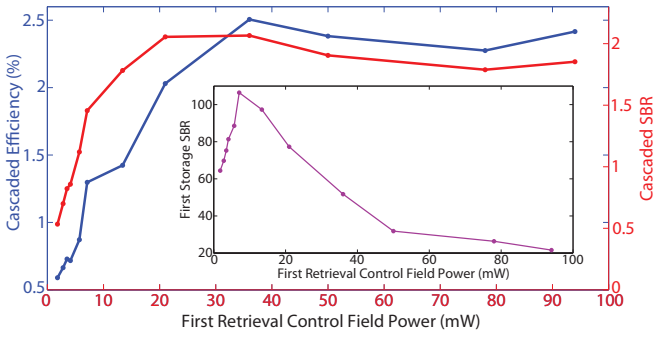

FIG. 5: (color online) Total cascaded storage efficiency η_T (blue line with circles) and cascaded SBR (red line with diamonds) vs. optical power for first retrieval. Inset: SBR of first storage event vs. optical power for first retrieval.

Finally we turn our attention to the noise characteristics of our cascaded storage system. Specifically, we are interested in the influence of the background noise photons generated from the first optical storage event on the final cascaded storage signal. We have measured the cascaded storage efficiency (η_T), the cascaded SBR and the SBR of the first storage event vs. control field 1 power. We used input states containing an average of 18 photons per pulse and an on/off modulation.

We can see that the total SBR after the cascading event (solid red line in Fig. 5) follows the behavior of the total storage efficiency η_T (solid blue line in Fig. 5). By comparison, the SBR for the first storage event (see inset in Fig. 5) does not follow the SBR of the cascaded procedure. This indicates that the second EIT storage ensemble simultaneously serves as a filter of the background generated in the first storage ensemble, implying that filtering schemes are only needed at the point of final measurement. Similar built-in filtering techniques have been implemented in light-matter interfaces with different purposes [27, 28].

Creating a network of multiple devices that contain built-in filtering mechanisms will lead to a major decrease in both experimental overhead and overall loss in the end-point read-out signal and becomes a fundamental consideration when constructing many-device machines.

In summary, we have demonstrated the first cascaded storage of few-photon level pulses using two distinct atomic ensembles contained in the same vapor cell. Few photon-level operation is made possible, even when using non-perfect devices, by combining photon shaping techniques and built in filtering in the quantum light matter interfaces. We do mention that in our realization the few-photon *cascaded* efficiency is of the same magnitude as the *single-device* efficiency reported in recent implementations [29, 30]. Our results demonstrate that with current room temperature technology it is viable to interconnect several quantum light-matter interfaces in a sequential manner with minimal interconnection losses, a key attribute of a quantum optical network.

In our particular implementation it is not possible to use an original input at the single-photon level due to the non-unitary efficiencies of both systems and the inherent losses required by using a dual rail system. Significant improvement in efficiency and SBR are required in order to operate with single-photon carrying qubits. Some of this losses can be addressed by using separate vapor cells connected in series. Achieving this interconnection between quantum memories for input single photons carrying qubits could be a milestone towards building more sophisticated machines that interface even more quantum optical nodes. This in turn will pave the way for the creation of elementary one-way quantum information processors based on warm vapor ensembles.

This work was supported by the US-Navy Office of Naval Research, grant number N00141410801 (instrumentation) and the National Science Foundation, grant number PHY-1404398 (personnel and materials). C. K. acknowledges financial support from the Natural Sciences and Engineering Research Council of Canada.

[1] A. Reiserer and G. Rempe, arXiv:1412.2889v1 (2014).
[2] T. E. Northup and R. Blatt, Nature Photonics 8, 356 (2014).
[3] K. S. Choi, A. Goban, S. B. Papp, S. J. van Enk and H. J. Kimble, Nature 468, 412 (2010).
[4] S. Ritter, C. Noelleke, C. Hahn, A. Reiserer, A. Neuzner, M. Uphoff, M. Muecke, E. Figueroa, J. Bochmann and G. Rempe, Nature 484, 195 (2012).
[5] G. Vittorini, D. Hucul, I. V. Inlek, C. Crocker, and C. Monroe, Phys. Rev. A 90, 040302(R) (2014).
[6] L.-M. Duan and C. Monroe, Rev. Mod. Phys. 82, 1209 (2010).
[7] D. A. B. Miller, Nature Photonics 4, 3 (2010).
[8] H. J. Kimble, Nature 453, 1023 (2008).
[9] L. Huang and Y. C. Lai, Chaos 21, 025107 (2011).
[10] L. Fan, K. Y. Fong, M. Poot and H. X. Tang, Nature Communications 6, 5850 (2015).
[11] S. Perseguers, G. J. Lapeyre, D Cavalcanti, M. Lewenstein and A. Acin, Rep. Prog. Phys. 76, 096001 (2013).
[12] H. Krauter, D. Salart, C. A. Muschik, J. M. Petersen, Heng Shen, T. Fernholz and E. S. Polzik, Nature Physics 9, 400 (2013).
[13] J. Nunn,1, N. K. Langford, W. S. Kolthammer, T. F. M. Champion, M. R. Sprague, P. S. Michelberger, X.-M. Jin, D. G. England and I. A. Walmsley, Phys. Rev. Lett. 110, 133601 (2013).
[14] A. I. Lvovsky *et al.*, Nature Photonics 3, 706 (2009).
[15] F. Bussieres, N. Sangouard, M. Afzelius, H. de Riedmatten, C. Simon, W. Tittel, J. Mod. Opt. 60, 1519 (2013).
[16] C. Monroe, R. Raussendorf, A. Ruthven, K. R. Brown, P. Maunz, L.-M. Duan and J. Kim, Phys. Rev. A 89, 022317 (2014).
[17] X. F. Xu, X. H. Bao and J. W. Pan, Phys. Rev. A 86, 050304(R) (2012).
[18] G. T. Campbell, O. Pinel, M. Hosseini, T. C. Ralph, B. C. Buchler and P. K. Lam, Phys. Rev. Lett. 113, 063601 (2014).
[19] Y. Cai, J. Feng, H. Wang, G. Ferrini, X. Xu, J. Jing and N. Treps, arXiv:1410.3672v2 (2014).
[20] I. Novikova *et al.*, Laser and Photonics Reviews 6, 333 (2012).
[21] M. D. Eisaman et al., Nature 438, 837 (2005).
[22] M. R. Sprague, P. S. Michelberger, T.F.M.Champion, D.G.England, J.Nunn, X. M. Jin, W. S. Kolthammer, A. Abdolvand, P. St. J.Russell and I. A. Walmsley, Nature Photonics 8, 287 (2014).
[23] M. Hosseini, G. Campbell, B. M. Sparkes, P. K. Lam, and B. C. Buchler, Nature Physics, 7, 794 (2011).
[24] P. S. Michelberger, T. F. M. Champion, M. R. Sprague, K. T. Kaczmarek, M. Barbieri, X. M. Jin, D. G. England, W. S. Kolthammer, D. J. Saunders, J. Nunn and I. A. Walmsley, arXiv:1405.1470v1 (2014).
[25] D. G. England, K. A. G. Fisher, J.P. W. MacLean, P. J. Bustard, R. Lausten, K. J. Resch and B. J. Sussman, arXiv:1409.2892v2 (2014).
[26] C. Kupchak, T. Mittiga, B. Jordaan, M. Namazi, C. Noelleke and Eden Figueroa, *Scientific Reports* **5**, 7658 (2015).
[27] D. L. McAuslan, L. R. Taylor, and J. J. Longdell, App. Phys. Lett. 101, 191112 (2012).
[28] N. Maring, K. Kutluer, J. Cohen, M. Cristiani, M. Mazzera, P. M. Ledingham and H. de Riedmatten, New Journal of Physics 16, 113021 (2014).
[29] P. Jobez, C. Laplane, N. Timoney, N. Gisin, A. Ferrier, P. Goldner and M. Afzelius, arXiv:1501.03981 (2015).
[30] C. Sayrin, C. Clausen, B. Albrecht, P. Schneeweiss and A. Rauschenbeutel, Optica 2, 353 (2015).